

Open-loop control of a MEMS deformable mirror for large-amplitude wavefront control

Jason B. Stewart,^{1,*} Alioune Diouf,² Yaopeng Zhou,² and Thomas G. Bifano^{2,3}

¹*Department of Electrical and Computer Engineering, Boston University, 8 Saint Mary's Street, Boston, Massachusetts 02215, USA*

²*Department of Manufacturing Engineering, Boston University, 15 Saint Mary's Street, Brookline, Massachusetts 02446, USA*

³*Boston University Photonics Center, 8 Saint Mary's Street, Boston, Massachusetts 02215, USA*

*Corresponding author: jstew@bu.edu

Received July 12, 2007; revised September 19, 2007; accepted October 4, 2007;
posted October 15, 2007 (Doc. ID 84863); published November 29, 2007

A method is introduced for predicting control voltages that will generate a prescribed surface shape on a MEMS deformable mirror. The algorithm is based upon an analytical elastic model of the mirror membrane and an empirical electromechanical model of its actuators. It is computationally simple and inherently fast. Shapes at the limit of achievable mirror spatial frequencies with up to 1.5 μm amplitudes have been achieved with less than 15 nm rms error. © 2007 Optical Society of America

OCIS codes: 230.4040, 010.1080, 230.6120, 110.6770, 170.4460, 000.2170.

1. INTRODUCTION

The use of microelectromechanical systems (MEMS) deformable mirrors (DMs) for wavefront control in adaptive optics (AO) systems is primarily motivated by their high actuator density and low cost, which is about ten times better than conventional technology [1]. MEMS-based DMs have also demonstrated subnanometer positioning precision, repeatability, and stability, making them very attractive options for high-contrast astronomical imaging, vision science, and microscopy applications [1–4].

Controlling a continuous facesheet DM through actuation at discrete points is complicated by the fact that actuators are mechanically coupled to one another through the mirror facesheet [5]. As a result, the displacement of any DM actuator alters the forces experienced by its neighboring actuators. This phenomenon is common to all continuous facesheet DMs and the degree of mechanical coupling is often characterized by an influence function, which is the ratio of displacement of the DM at an unenergized actuator location to that of the DM at an adjacent energized actuator location. Due to this mechanical coupling between adjacent actuators, closed-loop control is generally used to achieve highly accurate wavefront corrective shapes.

In closed-loop control a desired mirror shape is achieved iteratively by measuring wavefront phase errors and then using these measurements as feedback to change DM actuator control voltages [3–7]. Using MEMS DM technology, residual wavefront errors of better than 1 nm rms within the control band of the mirror have been reported [8]. Although closed-loop control is adequate for some AO applications, it is problematic for others. For example, in light-starved systems, splitting a beam to per-

form wavefront sensing worsens the signal-to-noise ratio of the image. Also, in AO systems that require high-speed performance, the control's iterative approach limits system bandwidth. Finally, there are some applications for which closed-loop DM control is simply not viable. For example, in future extremely large telescopes (ELTs), multiobject adaptive optics (MOAO) has been proposed as a way to correct wavefront phase errors over the entire telescope field of view [9]. This involves several wavefront sensing systems that are blind to their corresponding DMs. To achieve precise DM control in MOAO instruments, an open-loop controller is needed.

Development of an open-loop control algorithm for MEMS DM technology has been approached using empirical and mathematical models [10–13]. These algorithms were developed specifically to control MEMS DMs produced by Boston Micromachines Corporation (BMC). Morzinski *et al.* at the Laboratory for Adaptive Optics, University of California, Santa Cruz, developed the most accurate open-loop control routine reported thus far, which predicts DM control voltages for 500 nm amplitude mirror shapes with residual errors of ~ 15 nm rms [12].

The open-loop control algorithm presented here is based upon many of the same assumptions made in the aforementioned work. In particular it uses an empirical model to describe the behavior of the electrostatic actuator. Where this method differs is in its use of an analytical model to describe the loading and deflection of the mirror surface, incorporating both mirror bending and stretching behavior. Using these two models the control voltages for a desired mirror shape are predicted in a single control iteration that involves relatively low computation complexity. Mirror shapes with deflection amplitudes of the order

of 1.5 μm , as well as shapes at the limit of achievable DM spatial frequencies, have been predicted with better than 15 nm rms accuracy.

2. DEVICE

A. Architecture

Commercial MEMS DMs based on the devices pioneered at Boston University (BU) have up to 1024 electrostatically controlled actuators (32×32), corresponding to a total aperture size of ~ 10 mm. They have the ability to modulate the spatial and temporal features of an optical wavefront over a range of several micrometers with nanometer-scale repeatability [14,15]. Mirror surface flatness is limited by the microfabrication process and is of the order of 13 nm rms [8].

DMs are fabricated at a MEMS foundry using a 6'' wafer-scale three-layer polycrystalline silicon (polysilicon) surface micromachining process that uses phosphosilicate glass (PSG) as a sacrificial material. DMs are also diced and released at the foundry. Mirrors are deformed using surface normal electrostatic actuators (Fig. 1). The actuators are comprised of a compliant electrode diaphragm (second polysilicon layer) supported along two edges above a fixed electrode (first polysilicon layer). The top surface of the actuator diaphragm is connected to the mirror surface (third polysilicon layer) by an anchoring post at its center. The mirror reflectivity is enhanced with a gold or aluminum coating deposited on the final polysilicon layer.

A 300 μm pitch DM with 2 μm stroke and 144 actuators (12×12) was selected to demonstrate the open-loop control method presented here. The DM has an aperture width of 3.3 mm and a facesheet thickness of 3 $\mu\text{m} \pm 5\%$. The actuator diaphragm is 2 $\mu\text{m} \pm 5\%$ thick, 230 μm wide and has a 260 μm span.

B. Model

The open-loop control algorithm is based upon a DM model that consists of two coupled mechanical subsystems: the continuous facesheet and the array of actuators connected to the facesheet via rigid posts. The control algorithm determines the forces involved in this system through an equilibrium force balance at the posts, which are the points of connection for the two subsystems. This can be seen in the free body diagram of Fig. 2, where F_M corresponds to the force imparted to the mirror post by the elastic displacement of the mirror facesheet, F_A is the force associated with the elastic displacement of the actuator diaphragm, and F_E is the electrostatic force asso-

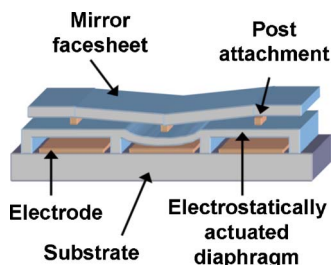


Fig. 1. (Color online) Continuous facesheet MEMS DM technology.

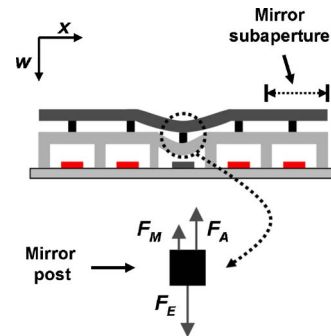


Fig. 2. (Color online) Cross section of an actuated DM subaperture (top) and free body diagram for its post (bottom). F_M is the mirror force, F_A is the actuator restoring force, and F_E is the applied electrostatic force.

ciated with an applied actuator voltage. The mirror area over an actuator is referred to as a mirror subaperture.

The DM facesheet is modeled as a thin plate free on all edges undergoing both stretching and bending [16,17]. Mirror deformation varies continuously in both the x and y directions. For displacements smaller than the facesheet thickness, the deformation is dominated by linear elastic bending as described by the biharmonic thin plate equation, which assumes negligible in-plane strain (Timoshenko and Woinowsky-Krieger [16], p. 82, Eq. 103):

$$\nabla^4 w(x,y) = \frac{q(x,y)}{D}, \quad (1)$$

where $q(x,y)$ is the surface normal distributed load (N/m^2) responsible for producing mirror facesheet deflection $w(x,y)$, and D is the plate flexural rigidity, given by

$$D = \frac{Eh^3}{12(1-\nu^2)}, \quad (2)$$

where E is Young's modulus, ν is Poisson's ratio, and h is the facesheet thickness. As displacement approaches the thickness of the facesheet, in-plane strain is no longer negligible and the facesheet begins to stretch as well as bend. This requires the inclusion of a nonlinear stretching term in Eq. (1) (Timoshenko and Woinowsky-Krieger [16], p. 378, Eq. 217):

$$\nabla^4 w(x,y) = \frac{q(x,y)}{D} + \frac{6}{h^2} \left\{ \left[\left(\frac{\partial w(x,y)}{\partial x} \right)^2 \frac{\partial^2 w(x,y)}{\partial x^2} \right] + \left[\left(\frac{\partial w(x,y)}{\partial y} \right)^2 \frac{\partial^2 w(x,y)}{\partial y^2} \right] \right\}. \quad (3)$$

Equation (3) is the governing equation for out-of-plane deflections of a linear elastic plate experiencing bending and stretching. It assumes that the mirror facesheet only experiences surface normal forces and that any lateral forces can be neglected. It also assumes that there are no initial internal stresses in the facesheet. Using this equation the generalized load $q(x,y)$ necessary to create a desired (known) mirror shape $w(x,y)$ can be calculated. In reality, however, the mirror is loaded only at discrete points corresponding to the mirror post locations, and the generalized load can be represented by a collection of discrete forces F_M acting at these post locations. F_M is esti-

mated at each post by integrating $q(x,y)$ over each DM subaperture, as shown in Fig. 3.

The electrostatically driven actuators are the second subsystem of the DM model. Although they are modeled empirically in the open-loop control algorithm, it is useful to first review approximate analytical models that describe their behavior. To a first order the actuators can be modeled as a parallel-plate spring system (Fig. 4). The top plate represents the compliant actuator diaphragm, which is attached to a spring representing the restoring force associated with its elastic displacement. The bottom plate represents the actuator's fixed electrode. In this model it is assumed that the plate representing the actuator diaphragm is infinitely rigid and that its stiffness is constant, similar to a linear spring.

With the application of a voltage between the actuator diaphragm and its electrode, an electrostatic force F_E is imparted to the diaphragm causing it to deflect. Assuming the lateral dimensions of the parallel plates representing the actuator are much greater than their separation, F_E can be determined analytically to be

$$F_E = \frac{\epsilon_0 A V^2}{2(g_0 - w_p)^2}, \quad (4)$$

where ϵ_0 is the permittivity of free space, A is the plate area, V is the applied voltage, g_0 is the initial plate separation, and w_p is the plate displacement [18]. Assuming constant stiffness k_A , the actuator deflection creates a mechanical restoring force F_A at the mirror post that is proportional to the displacement of the actuator w_p :

$$F_A = k_A w_p. \quad (5)$$

To use this analytical model for the actuator subsystem in an open-loop control algorithm, one could perform a static equilibrium force balance at each actuator's centrally located post, with the simplifying assumption that the electrostatic force acts at a point instead of being distributed across the actuator plate. Balancing the forces for this model we find an analytical expression for actuator control voltages:

$$V_i = \sqrt{\frac{2(g_0 - w_{p,i})^2(k_A w_{p,i} + F_{M,i})}{\epsilon_0 A}}, \quad (6)$$

where the subscript i identifies a particular actuator. This demonstrates the dependence of actuator control voltage on its displacement *and* on forces coupled from the DM facesheet.

Unfortunately, the parallel-plate electrostatic model [Eq. (4)] and linear-spring mechanical model [Eq. (5)] pro-

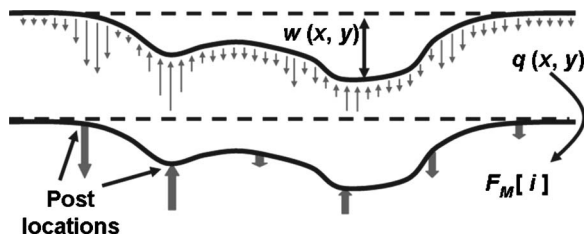


Fig. 3. Estimating mirror forces $F_{M[i]}$ from generalized surface-normal mirror load $q(x,y)$.

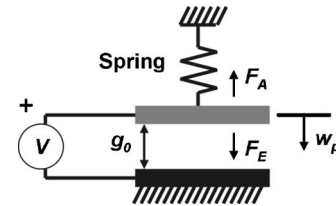


Fig. 4. Simplified parallel-plate and linear-spring actuator model.

vide relatively poor approximations of the actuator behavior. The actuator diaphragm is rigidly fixed along two opposing edges and not free as the model assumes. Such actuator diaphragm boundary conditions are referred to as “fixed–fixed.” As a result the electrostatic model is limited by the fact that the electrodes are only parallel when the actuator is in its initial unenergized position. Therefore the electrostatic force distribution across the actuator diaphragm changes with increased deflection from one that is initially uniform to one that is concentrated near the diaphragm center. The mechanical model is also limited by stretching that effectively stiffens the actuator with increased deflection, i.e., k_A is not constant.

Open-loop control is still tractable, however, because the two forces F_A and F_E are local to the actuator, while global coupling is completely described through the mirror force F_M at each actuator post. Because of this, it is possible to reduce the open-loop control problem to one that is entirely local and uncoupled, provided that the mirror force F_M is known at each actuator. As a result, the electrostatic actuator response to a local mirror force F_M can be modeled through a compact set of empirical measurements with the functional relationship $F_M = f(w_p, V)$, which is subject to the equilibrium condition:

$$F_M = F_A + F_E. \quad (7)$$

The open-loop control approach presented here is therefore based on using a calibration step to find a local, empirical measure of the actuator behavior linking values of F_M , w_p , and V , where w_p now refers to the displacement of the actuator post connection.

3. OPEN-LOOP CONTROL

A. Method

Empirical characterization of the DM actuators consists of applying a variety of arbitrary shapes of known voltages to the mirror surface. The mirror shape $w(x,y)$ is then measured using a surface mapping interferometer. F_M is estimated by inserting $w(x,y)$ into Eq. (3) and integrating the load $q(x,y)$ around each actuator post, as discussed above. Knowledge of the mirror shape $w(x,y)$ also specifies w_p at each actuator post. A surface of the same functional form of Eq. (6) is fit to this data spanning $\{w_p, F_M, V\}$ via a least-squares fit routine. Thus for an arbitrary desired mirror shape $w(x,y)$, w_p is known, F_M is calculated, and $V(w_p, F_M)$ is calculated using predetermined surface coefficients.

The calibration table shown in Fig. 5 (right) was created by applying identical voltages to a ring of actuators (left) to vary F_M at the central actuator. $w_p(V)$ for the central actuator was then measured using a Zygo New View

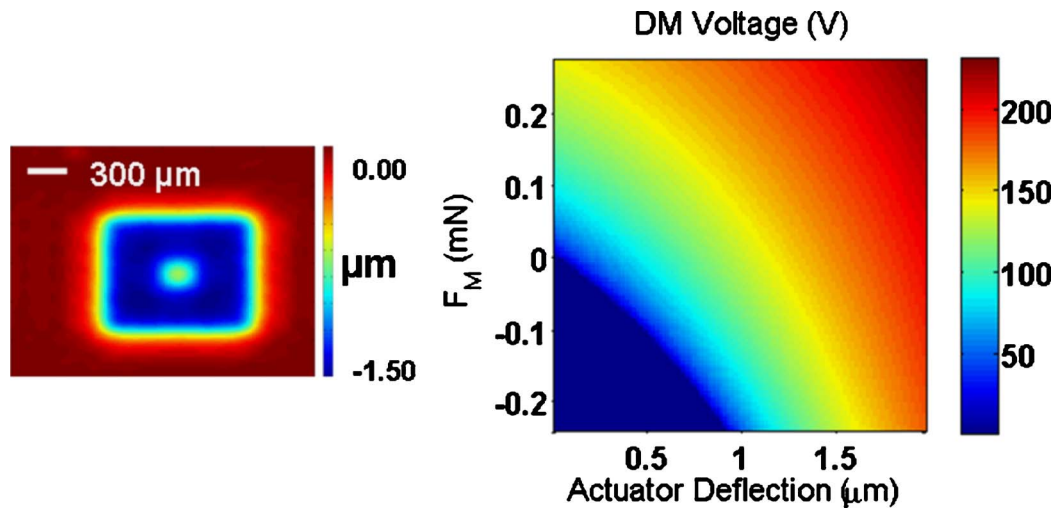


Fig. 5. (Color online) (Left) Shape used to calibrate DM. Identical voltages are applied to a ring of actuators to vary F_M at the central actuator. (Right) $w_p(V)$ for the central actuator is measured for different ring voltages to produce the calibration dataset spanning $\{w_p, F_M, V\}$. One-hundred data points from a single central actuator of the 12×12 DM were collected and fit to a surface of the same functional form as Eq. (6). Surface fitting error was 4 V rms.

6000 optical profiler for several ring voltages (or F_M 's). F_M was calculated at each actuator using Eq. (3). One-hundred data points for F_M , w_p , and V for a single actuator were recorded and used to predict the open-loop control voltages for the shapes presented below. The surface fit error for this calibration dataset was 4 V rms. Since the architecture of this DM is such that all actuators are nominally identical, it was assumed that calibration of one actuator will be sufficient to characterize all actuators. Consequently, geometrical and material variations across the actuator array result in controller errors.

For the results presented here, mirror deflections are referenced from an unenergized mirror shape, i.e., differential deflection. Unactuated peripheral surfaces of the DM are used to define a deflection reference plane, $w(x,y)=0$, during calibration. Once a reference plane is established, actuator displacement can be determined solely by knowing mirror facesheet displacement.

The open-loop control software is based in Matlab and performs all hardware communication and data analysis. The software controls an 8-bit high-voltage power supply and the Zygo NewView 6000 asynchronously to apply desired shapes to the DM and to record the surface shapes. The driver voltage resolution is ~ 1.2 V, which corresponds to less than 1 nm at low drive voltages and ~ 12 nm at the maximum drive voltage. F_M computation is performed using the Matlab discrete differentiation routines. The microscope magnification and CCD resolution used to view the full DM aperture determine the number of surface data points used in mirror calibration, which are approximately 300×300 pixels, corresponding to a field of view of approximately 3×3 mm. This surface data is low-pass filtered with a cutoff spatial frequency just greater than the maximum frequency controllable by the DM to reduce noise in the mirror load calculations.

B. Results

1. Evaluation of Open-Loop Control Algorithm

To demonstrate the open-loop DM control algorithm, we begin by using a previously measured surface map of the

DM as the desired mirror shape, $w(x,y)$, which has a single energized actuator deflected by $\sim 1 \mu\text{m}$ (Fig. 6). Controlling to a previously measured DM mirror shape ensures that the desired control target shape is achievable. Figure 6 shows the desired mirror shape $w(x,y)$ from which mirror pressure $q(x,y)$ is determined via Eq. (3). From these two datasets, the mirror post displacement w_p and mirror forces F_M at the posts are determined, allowing the prediction of the control voltage using the calibration surface in Fig. 5. The predicted open-loop voltage for the array corresponds closely with the voltage used to generate the reference shape and is within the 4 V fitting error of the calibration surface.

In a subsequent, more challenging control exercise, a $1.5 \mu\text{m}$ amplitude stripe pattern was used for the desired shape, as shown in Fig. 7. Again, this target shape was obtained by previously measuring the mirror surface when every other column of actuators was energized, producing a shape that pushes the upper limit of the DM's achievable spatial frequencies. The residual shape error after open-loop control was 13.5 nm rms.

A third test of open-loop control performance was to compare it to that of closed-loop control for an ideal, mathematically defined target shape. To do this a closed-loop control routine was employed that used measured Zygo interferometric surface map data as feedback. An ideal section of spherical surface with an approximately 800 mm radius of curvature ($1.5 \mu\text{m}$ peak-to-valley across the active DM aperture) was used as the reference shape for both control routines. These results are shown in Fig. 8. The residual error between the ideal shape and the closed-loop controlled shape was 36.7 nm rms, and for the open-loop controlled shape was 41.0 nm rms.

2. Evaluation of Actuator Mechanics

For the linear spring model discussed in Subsection 2.B, k_A in Eq. (5) corresponds to the stiffness of the actuator diaphragm, which is assumed to be constant. If the actuator diaphragm is modeled as a fixed-fixed beam under a central point load, its stiffness can be found analytically

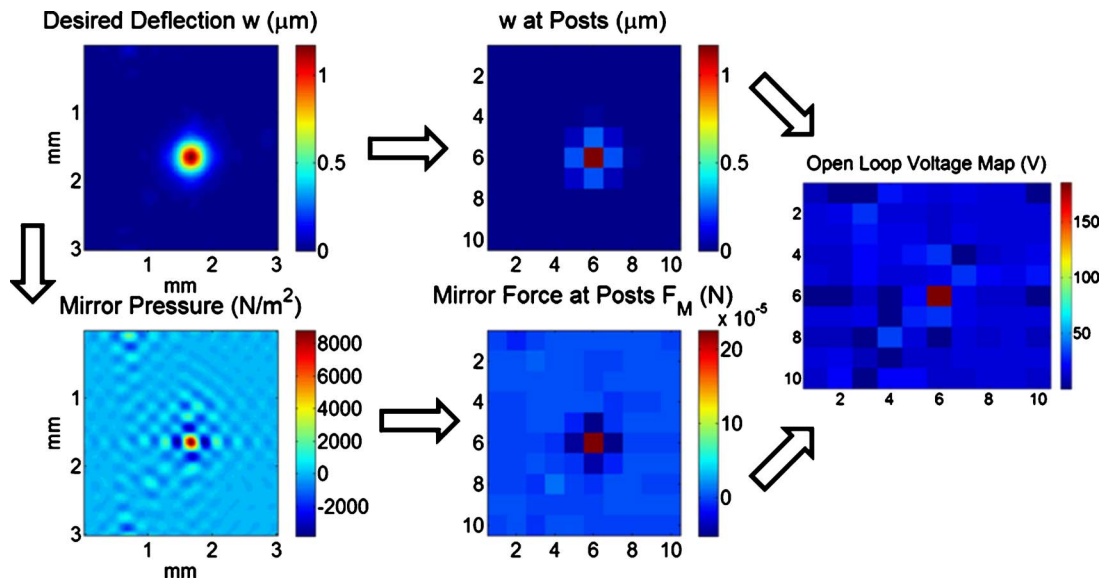


Fig. 6. (Color online) Demonstration of DM open-loop control. The difference between the actual and predicted voltages for the deflected actuator was less than the calibration surface fitting error, 4 V rms.

using $16ESh_A^3/L^3$, where h_A is the diaphragm thickness, S is its width and L is its length [19]. Plugging in dimensions for the actuator used in these experiments, a constant stiffness value of approximately 190 N/m is found (Fig. 9, dashed line).

However, in reality k_A depends on both the distribution of the loading force as well as the magnitude of its displacement due to stretching. If an actuator diaphragm is loaded only by the mirror through adjacent actuator coupling, but remains itself unenergized ($F_E=0$), the force balance equation becomes $F_M=F_A=k_A w_p$ [Eqs. (5) and (7)], from which k_A can be determined from the $V=0$ slice of the calibration surface in Fig. 5 (Fig. 9, squares). The fact that k_A increases with w_p suggests that the actuator in fact experiences stretching as it is deflected. To corroborate this physical result, the empirically derived actuator stiffness was compared to stiffness data measured using a Hysitron TriboIndenter, which applies a known point load while recording deflection. In this experiment the point load is applied to the actuator at the post location, with no mirror attached. k_A corresponds to the slope of this curve. The results of several measurements from a stand-alone actuator near the DM perimeter can be seen in Fig. 9 (circles).

For a given actuator displacement, we see that the measured actuator stiffness is very close to the empiri-

cally derived stiffness. This suggests that the mirror forces estimated from the mirror facesheet analytical model (used in the empirical actuator calibration) are relatively accurate. The dependence of actuator stiffness on displacement is also evident in the TriboIndenter results. The discrepancy between the derived stiffness and measured stiffness could be due to an overestimation of F_M from the DM facesheet load $q(x,y)$.

4. DISCUSSION

The open-loop control method proved successful in allowing accurate control of the DM surface in a single iteration, based on a sparse calibration procedure and a computationally efficient algorithm. Evaluation of the control algorithm for higher-order Zernike shapes, larger stroke DMs, as well as devices with up to 1024 actuators is under way. The behavior of devices with higher actuator counts is not expected to reduce control accuracy.

As mentioned above, the results presented here are for differential mirror deflection measurements, i.e., when the mirror displacement is referenced from its 0 V initial shape. The control algorithm also assumes actuator uniformity throughout the DM. In reality the initial DM surface is seldom perfectly flat at 0 V due to residual stress in the mirror facesheet and polishing errors. Further-

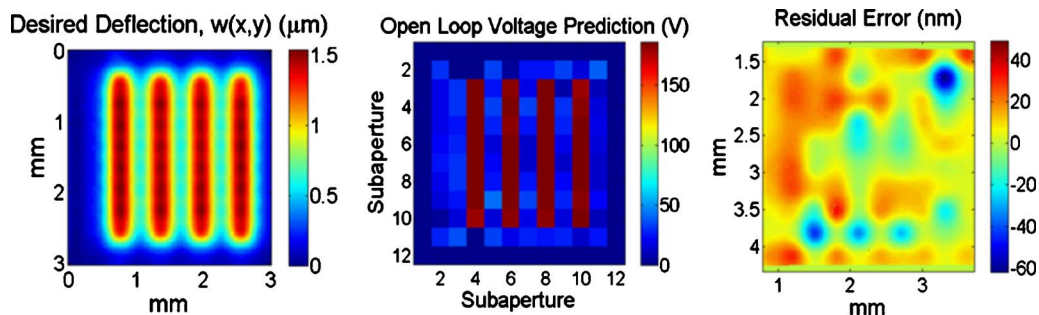


Fig. 7. (Color online) (Left) Open-loop voltage prediction for a 1.5 μm amplitude (185 V) stripe pattern. (Center) Predicted voltage map and (right) residual errors between desired and predicted shapes, with 111 nm peak-to-valley and 13.5 nm rms error.

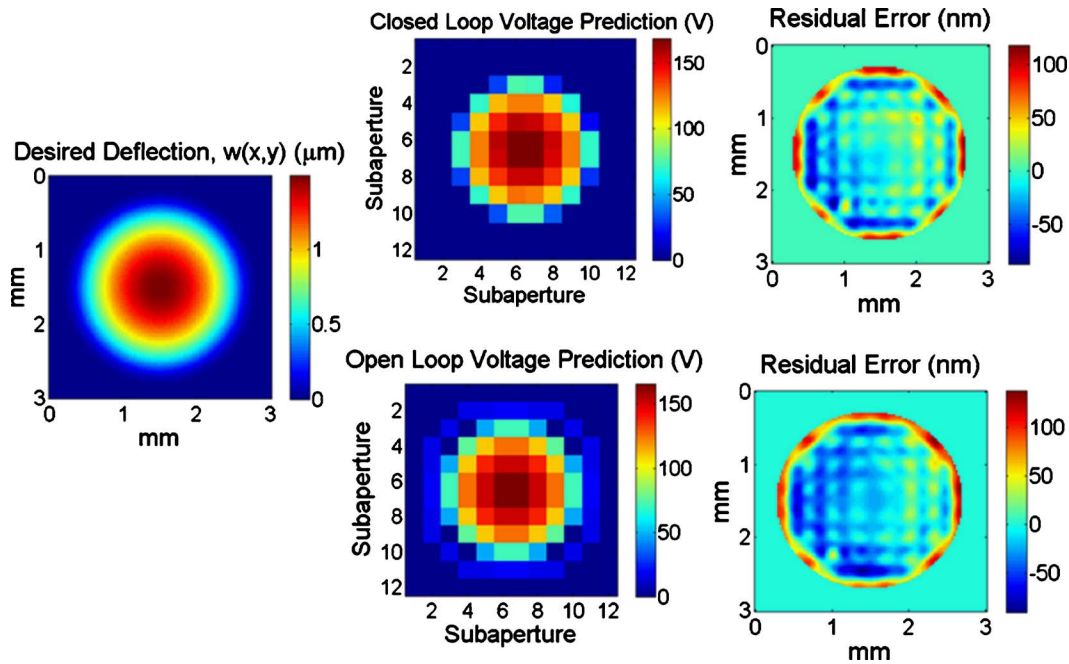


Fig. 8. (Color online) (Left) Open-loop and closed-loop voltage maps for ideal focus shift Zernike. (Top center) Closed-loop voltage map and (top right) residual errors between desired and achieved shapes (206 nm peak-to-valley and 36.7 nm rms). (Bottom center) Open-loop voltage map and (bottom right) residual errors between desired and predicted shapes (228 nm peak-to-valley and 41 nm rms).

more, tolerances in the manufacturing process lead to large nonuniformities in actuator mechanical properties across the array, which affects overall system accuracy. These nonuniformities may be the primary cause for the residual errors discussed in Subsection 3.B.1.

One method for addressing these nonuniformities is to perform a more complete empirical calibration of the DM, evaluating more actuators across the array at more points per actuator. Another solution is to incorporate these nonuniformities into the analytical model for the control algorithm, which is a topic currently being explored. For ex-

ample, knowledge of the initial stress in the mirror facesheet could be incorporated into the calculations for F_M .

The use of an empirical model for the description of actuator mechanics is robust because it incorporates some of these nonuniformities in the calibration procedure. For example, the constants of the biharmonic plate equation (3) can vary substantially, such as flexural rigidity, where Young's modulus and polysilicon layer thicknesses are uncertain to $\sim 5\%$. Furthermore, it allows continued use of the algorithm even when actuator designs change, which is not easy to accommodate in purely mathematical or analytical models.

5. SUMMARY

An open-loop control algorithm for predicting the control voltages of desired mirror shapes has been demonstrated. Shapes with deflection amplitudes of the order of $1.5 \mu\text{m}$ and at the limit of achievable DM spatial frequencies have been achieved with better than 15 nm rms accuracy. The algorithm uses an analytical model to describe the loading and deflection of the DM surface and an empirical model to describe the behavior of the electrostatic actuators. The analytical model of the plate is used to obtain the load necessary to create a desired mirror shape. The empirical model is constructed by applying a variety of arbitrary shapes of known voltages and computed mirror forces at the posts. A least-square linear fit of the set $\{w_p, F_M, V\}$ produces the empirical surface used for voltage prediction. This method circumvents the shortcomings associated with using a parallel-plate actuator model and a linear-spring mechanical model.

ACKNOWLEDGMENTS

Portions of this work were supported by Army Research Laboratory contract W911NF-06-2-0040. Mirrors were

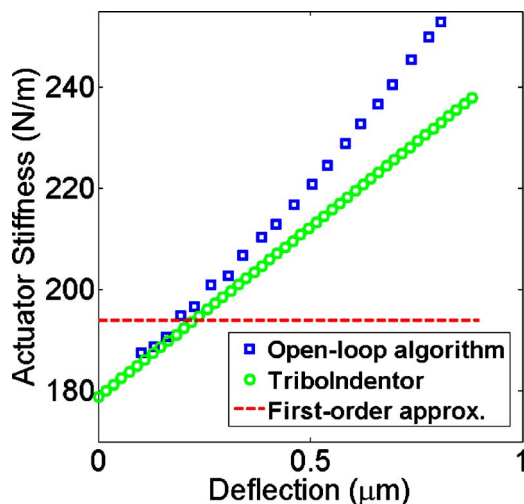


Fig. 9. (Color online) Actuator mechanical stiffness under central point load. The agreement between the empirically derived actuator stiffness (squares) and the TriboIndenter measured stiffness (circles) suggests the analytical model used for describing plate deformation is accurate. Actuator stiffness is also compared to a first-order analytical fixed-fixed beam approximation (dashed line), which does not account for actuator stretching behavior.

provided by Boston Micromachines Corporation. T. G. Bifano acknowledges a financial interest in Boston Micromachines Corporation. The authors are grateful for support from D. Gavel and K. Morzinski and for experiments performed by Janice Castillo and Andrew Legendre.

REFERENCES

1. M. E. Motamedi, *MOEMS-Micro-Opto-Electro-Mechanical Systems* (SPIE Press, 2005).
2. K. M. Morzinski, J. W. Evans, S. Severson, B. Macintosh, D. Dillon, D. Gavel, C. Max, and D. Palmer, "Characterizing the potential of MEMS deformable mirrors for astronomical adaptive optics," *Proc. SPIE* **6272**, 627221 (2006).
3. E. J. Fernández and P. Artal, "Membrane deformable mirror for adaptive optics: performance limits in visual optics," *Opt. Express* **11**, 1056–1069 (2003).
4. Y. Zhou and T. Bifano, "Characterization of contour shapes achievable with a MEMS deformable mirror," *Proc. SPIE* **6113**, 123–130 (2006).
5. F. Roddier, *Adaptive Optics in Astronomy* (Cambridge U. Press, 1999), pp. 77–80.
6. J. M. Beckers, "Adaptive optics for astronomy: principles, performance, and applications," *Annu. Rev. Astron. Astrophys.* **31**, 13–62 (1993).
7. J. Hardy, *Adaptive Optics for Astronomical Telescopes* (Oxford U. Press, 1998).
8. J. W. Evans, B. Macintosh, L. Poyneer, K. Morzinski, S. Severson, D. Dillon, D. Gavel, and L. Reza, "Demonstrating sub-nm closed loop MEMS flattening," *Opt. Express* **14**, 5558 (2006).
9. D. T. Gavel, "Adaptive optics control strategies for extremely large telescopes," *Proc. SPIE* **4494**, 215–220 (2002).
10. Y. Zhou and T. Bifano, "Adaptive optics using a MEMS deformable mirror," *Proc. SPIE* **6018**, 350–356 (2005).
11. C. R. Vogel and Q. Yang, "Modeling, simulation, and open-loop control of a continuous facesheet MEMS deformable mirror," *J. Opt. Soc. Am. A* **23**, 1074–1081 (2006).
12. K. M. Morzinski, K. B. W. Harpsee, D. T. Gavel, and S. M. Ammons, "The open loop control of MEMS: modeling and experimental results," *Proc. SPIE* **6467**, 64670G (2007).
13. M. H. Miller, J. A. Perrault, G. G. Parker, B. P. Bettig, and T. G. Bifano, "Simple models for piston-type micromirror behavior," *J. Micromech. Microeng.* **16**, 303–313 (2006).
14. T. G. Bifano, R. Mali, J. Perreault, K. Dorton, N. Vandelli, M. Horentein, and D. Castanon, "Continuous membrane, surface micromachined silicon deformable mirror," *Opt. Eng. (Bellingham)* **36**, 1354–1360 (1997).
15. T. G. Bifano, J. Perreault, R. K. Mali, and M. N. Horenstein, "Microelectromechanical deformable mirrors," *IEEE J. Sel. Top. Quantum Electron.* **5**, 83–90 (1999).
16. S. Timoshenko and S. Woinowsky-Krieger, *Theory of Plates and Shells* (McGraw-Hill, 1976), pp. 79–104 and 378–428.
17. A. Papavasiliou, S. Olivier, T. Barbee, C. Walton, and M. Cohn, "MEMS actuated deformable mirror," *Proc. SPIE* **6113**, 190–199 (2006).
18. S. D. Senturia, *Microsystem Design* (Springer Science, 2001), p. 134.
19. R. J. Roark and W. C. Young, *Formulas for Stress and Strain* (McGraw-Hill, 1982), p. 97.